Communications Earth & Environment

Supplementary Information for

Organic ligands in whale excrement support iron availability and reduce copper toxicity to the surface ocean.

Patrick J. Monreal[1,2], Matthew S. Savoca[3], Lydia Babcock-Adams[4], Laura E. Moore[1], Angel Ruacho[1], Dylan Hull[1], Logan J. Pallin[5], Ross C. Nichols[5], John Calambokidis[6], Joseph A. Resing[1,7,8], Ari S. Friedlaender[5], Jeremy Goldbogen[3], Randelle M. Bundy[1]

[1]School of Oceanography, University of Washington, Seattle, WA, USA
[2]Astrobiology Program, University of Washington, Seattle, WA, USA
[3]Hopkins Marine Station, Stanford University, Pacific Grove, CA, USA
[4]National High Magnetic Field Laboratory, Florida State University, Tallahassee, FL, USA
[5]Department of Ocean Sciences and Institute for Marine Science, University of California Santa Cruz, Santa Cruz, CA, USA
[6]Cascadia Research Collective, Olympia, WA, USA
[7]Cooperative Institute for Climate, Ocean, and Ecosystem Studies, University of Washington, Seattle, WA, USA
[8]Pacific Marine Environmental Laboratory, National Oceanic and Atmospheric Administration, Seattle, WA, USA

Contents of this file

Introduction

The following document includes all supplementary material cited in the manuscript, including tables and figures. First, (Supplementary Table 1) a table of the quantitative data from main text Figure 1, (Supplementary Table 2) a table of additional data on the L_2 and L_4 ligand pools for Fe, (Supplementary Table 3) a table of the copper ligand *m/z*'s, retention times, peak areas, and putative formulae, (Supplementary Table 4) a table of the scores of predicted molecular formulae, and (Supplementary Table 5) a table outlining key parameters used in voltammetry experiments. Then, eleven supplementary figures are included: (Supplementary Fig. 1) LC-ICP-MS chromatogram for ^{56}Fe, (Supplementary Fig. 2) voltammograms from competitive ligand exchange adsorptive cathodic stripping voltammetry (CLE-ACSV) experiments with iron, (Supplementary Fig. 3) voltammograms from standard addition of Suwannee River Humic Acid (SRHA) Standard III, (Supplementary Fig. 4) a photo of the 0.2 μm-filtered fecal samples, (Supplementary Fig. 5) MS1 spectra of a copper ligand with multiple peaks, (Supplementary Fig. 6) MS2 spectra of select copper ligands with preliminary annotations from *in-silico* fragmentation of known tetrapyrroles, (Supplementary Fig. 7) structures of example linear tetrapyrroles, (Supplementary Fig. 8) extracted ion chromatograms for *m/z*'s corresponding to domoic acid, (Supplementary Fig. 9) maps of approximate sampling locations, (Supplementary Fig. 10) voltammograms of CLE-ACSV experiments with copper, and (Supplementary Fig. 11) ferrioxamine E standard curve. Unless stated otherwise, plots were generated in RStudio.

Supporting Tables

Supplementary Table 1. Data from Figure 1 of the main text. Methods for each measurement are also found in the main text. $[L_{Fe}]_{CSV}$ (total ligand) includes both L_2 and L_4 ligands. Conditional stability constants and concentrations of each respective Fe ligand pool can be found in Supplementary Table 2.

Sample ID	Species	Region	Filtrate Physical Description	[dFe] (μM) ± 1SD	$[L_{Fe}]_{CSV}$ (μM eq Fe) ± SE (95% CI)	[eHS] (μM eq Fe range based on SRHA)	[Fe′] (nM) ± SE (95% CI)	$[Fe\text{-}L]_{SPE}$ (μM) *(assuming 5%–40% efficiency)*	$[pFe]_{labile}$ (mmol/kg dry weight) ± SE	Fe:P (mmol Fe/ mol P) ± SE
MN19	*M. novaeangliae*	Antarctic Peninsula	dark brown/ viscous	0.978 ± 0.200	423.7 ± 49.5	100.3–219.8	0.228 ± 0.167	0.141 (2.60–0.353)	1.41 ± 0.04	0.467 ± 0.027
MN20	*M. novaeangliae*	Antarctic Peninsula	light pink/orange	0.402 ± 0.167	100.2 ± 11.7	7.44–16.31	0.096 ± 0.021	0.0273 (0.497–0.068)	0.749 ± 0.05	0.356 ± 0.029
CRC7	*B. musculus*	California Current	light pink/clear	0.238 ± 0.091	190.5 ± 33.2	4.72–10.34	0.083 ± 0.028	-	-	-
CRC210	*B. musculus*	California Current	light brown	1.23 ± 0.250	644.6 ± 91.0	65.83–144.3	0.363 ± 0.267	-	-	-
MSS1	*B. musculus*	California Current	dark brown/ highly viscous	12.63 ± 1.88	211.7 ± 25.3	440.7–966.0	0.518 ± 0.102	-	-	-
Sample ID	**Species**	**Region**	**Filtrate Physical Description**	**[dCu] (μM) ± 1SD**	**$[L_{Cu}]_{CSV}$ (μM eq Cu) ± SE (95% CI)**	**$\log K^{cond}_{CuL,Cu'}$ ± SE (95% CI)**	**[Cu′] (pM) ± SE (95% CI)**	**$[Cu\text{-}L]_{SPE}$ (μM) *(assuming 5%–40% efficiency)***	**$[pCu]_{labile}$ (mmol/kg dry weight) ± 1SD**	**Cu:P (mmol Cu/ mol P) ± 1SD**
MN19	*M. novaeangliae*	Antarctic Peninsula	dark brown; viscous	221.0 ± 57.30	307.7 ± 16.12	14.47 ± 0.09	4.25 ± 1.54	4.90 (89.12–12.25)	3.13 ± 0.10	0.602 ± 0.041
MN20	*M. novaeangliae*	Antarctic Peninsula	light pink/orange	52.34 ± 1.74	66.93 ± 12.63	14.38 ± 0.04	2.21 ± 0.32	1.15 (20.97–2.88)	4.68 ± 0.09	1.29 ± 0.078
CRC7	*B. musculus*	California Current	light pink/clear	4.75 ± 0.80	-	-	-	-	-	-
CRC210	*B. musculus*	California Current	light brown	41.01 ± 5.59	-	-	-	-	-	-
MSS1	*B. musculus*	California Current	dark brown; highly viscous	121.7 ± 47.60	-	-	-	-	-	-

Supplementary Table 2. Additional data on L_2 and L_4 ligand pools for Fe from Figure 1 of the main text. The best-fit complexation models for each sample included two ligand groups, L_4 and L_2, with properties given below. These speciation calculations were conducted with ProMCC[1] and then corrected by a dilution factor according to how much sample was used in the titration vials (Supplementary Table 5). While titrations were at the edge of the detection window[2], the large array of analyses performed on these samples (e.g., [eHS] quantification, LC-ICP-MS, LC-ESI-MS, and LC-FT-ICR-MS) add confidence to measurements and agree with associated findings. Higher side reaction coefficients (α_{FeL}) for the L_2 pool suggest that the dFe is preferentially bound to the intermediate-strength humic-like class of ligands in the fecal matter.

Sample ID	$[L_4]_{CSV}$ (μM eq Fe) ± SE (95% CI)	$\log K^{cond}_{FeL_4,Fe'}$ ± SE (95% CI)	$\log \alpha_{FeL_4}$	$[L_2]_{CSV}$ (μM eq Fe) ± SE (95% CI)	$\log K^{cond}_{FeL_2,Fe'}$ ± SE (95% CI)	$\log \alpha_{FeL_2}$
MN19	413.2 ± 47.7	9.18 ± 0.06	5.80	10.48 ± 1.75	11.36 ± 0.28	6.38
MN20	97.7 ± 11.6	8.76 ± 0.06	4.75	2.42 ± 0.13	11.67 ± 0.06	6.06
CRC7	189.4 ± 33.1	8.20 ± 0.09	4.47	1.07 ± 0.09	11.89 ± 0.10	5.92
CRC210	633.5 ± 88.7	8.92 ± 0.07	5.72	11.02 ± 2.35	11.24 ± 0.25	6.28
MSS1	168.0 ± 23.5	9.65 ± 0.07	5.87	43.74 ± 1.75	11.69 ± 0.06	7.33

Supplementary Table 3. Cu ligands identified in fecal samples MN19 and MN20. Untargeted searches probing *m/z*'s for metal isotopologues with Δ*m/z* = 1.998192 and intensity ratios equal to the natural abundance ratio of $^{63}Cu/^{65}Cu$ were conducted on mass spectrometry data from sample MN19 (Methods). LC-ICP-MS retention times refer to peaks detected by that method (Fig. 2A) while concentrations refer to quantification by that method. LC-ESI-MS retention times are listed under each LC-ICP-MS peak to refer to Cu ligand peaks that were detected on the Q Exactive Orbitrap with similar retention times. Because FT-ICR-MS at the 21 Tesla facility has a higher resolving power, exact masses for each peak are listed from that data. Exact masses as well as intensities of ^{65}Cu-, ^{13}C-, ^{15}N-, ^{18}O-, and ^{34}S-isotopologues (if present) were used to determine the putative molecular formula of the compound using Freestyle (Thermo Scientific). If there were too few detectable isotopologue peaks and/or too many reasonable possibilities, no putative molecular formula was recorded. Even if no molecular formula was proposed, there is a high degree of confidence that all reported *m/z*'s are Cu-containing, based on very low Cu isotope error, referring to the difference between the measured Δ*m/z* for Cu isotopologue peaks and 1.998192, the exact Δ*m/z*. The magnitude of the Cu isotope error for almost every candidate ligand was below 0.1 mDa, averaging 0.028 mDa. Sample MN20 was also searched in a targeted approach for candidate ligands that were identified in MN19 to see what compounds were shared between them, and many were. In-depth structural characterization of the ligand pools of each sample was outside the scope this work, and volume limited some analyses.

LC-ICP-MS Retention Time (min)	Ferrioxamine E-based Concentration (nM)	LC-ESI-MS Retention Time (min)	FT-ICR-MS^3 Mass-to-Charge (m/z)	Predicted Molecular Ion Formula	Cu Isotope Error (mDa)	LC-ESI-MS Peak Area (a.u.)	Present in MN20?
14.74	**57.46**						
15.50	**31.10**						
17.32	**27.11**						
		17.55	783.29739	-	-0.012	1.36E+04	✗
		17.40	813.30782	-	0.018	1.30E+04	✗
18.08	**59.61**						
		17.90	685.28562	$[C_{29}H_{48}O_8N_7Cu]^+$	-0.012	1.75E+05	✓
20.27	**23.27**						
		20.27	728.24809	$[C_{35}H_{45}O_9N_4Cu]^+$	-0.002	6.12E+04	✗
		20.27	731.24491	-	-0.002	3.52E+04	✓
20.98	**23.83**						
		21.25	698.23728	$[C_{34}H_{43}O_8N_4Cu]^+$	0.008	2.41E+05	✓
		21.40	653.31888	-	-0.292	2.39E+05	✓
22.91	**13.04**						
		22.90	728.24795	-	0.018	2.64E+04	✗
23.53	**25.15**						
		23.65	879.26836	-	-0.032	1.46E+05	✗
		23.85	529.16326	$[C_{26}H_{32}O_5N_3Cu]^+$	-0.022	1.15E+05	✗
24.55	**34.16**						
		24.75	714.21466	$[C_{34}H_{43}O_7N_4SCu]^+$	0.008	7.61E+05	✓
		24.80	800.26901	$[C_{38}H_{49}O_{11}N_4Cu]^+$	-0.012	5.54E+05	✓
		24.30	670.24285	$[C_{33}H_{43}O_7N_4Cu]^+$	0.018	1.88E+05	✓
		24.90	710.24853	$[C_{34}H_{43}O_7N_6Cu]^+$	0.018	1.81E+05	✓
25.59	**66.14**						
		25.80	668.22670	$[C_{33}H_{41}O_7N_4Cu]^+$	0.008	1.18E+06	✓
		25.40	696.22161	$[C_{34}H_{41}O_8N_4Cu]^+$	-0.022	9.44E+05	✓
		25.59	654.24755	$[C_{33}H_{43}O_6N_4Cu]^+$	-0.012	6.07E+05	✓
		25.30	854.30640	$[C_{44}H_{51}O_8N_6Cu]^+$	0.018	2.58E+05	✓
		25.40	700.19892	$[C_{33}H_{41}O_7N_4SCu]^+$	-0.074	2.41E+05	✓
		25.59	940.37949	-	0.008	2.20E+05	✓
		25.40	694.20601	-	0.018	2.09E+05	✓
		25.59	819.32667	$[C_{42}H_{54}O_8N_5Cu]^+$	0.008	1.01E+05	✓
		25.40	731.23770	$[C_{37}H_{42}O_7N_5Cu]^+$	-0.012	9.22E+04	✓

		25.75	1000.36432	-	0.078	6.77E+04	✓
26.40	**42.40**						
		26.40	684.20469	$[C_{33}H_{41}O_6N_4SCu]^+$	-0.012	3.02E+06	✓
		26.15	684.25814	$[C_{34}H_{45}O_7N_4Cu]^+$	-0.012	2.02E+06	✓
		26.50	865.28931	$[C_{41}H_{52}O_8N_7SCu]^+$	0.028	1.34E+06	✓
		26.50	851.27366	$[C_{40}H_{50}O_8N_7SCu]^+$	-0.002	1.29E+06	✗
		26.46	650.21622	$[C_{40}H_{39}O_6N_4Cu]^+$	-0.002	3.69E+05	✗
		26.55	680.22677	$[C_{34}H_{41}O_7N_4Cu]^+$	-0.002	2.74E+05	✓
		26.35	699.21489	-	-0.012	1.01E+05	✗
		26.20	664.19569	$[C_{33}H_{37}O_7N_4Cu]^+$	0.028	8.84E+04	✓
27.19	**40.33**						
		27.10	682.24243	$[C_{34}H_{43}O_7N_4Cu]^+$	0.008	1.34E+06	✓
		27.25	984.36938	$[C_{50}H_{61}O_{11}N_6Cu]^+$	0.008	3.15E+05	✓
		27.30	716.23037	$[C_{34}H_{45}O_7N_4SCu]^+$	-0.002	2.86E+05	✗
28.42	**74.76**						
		28.42	698.21969	$[C_{34}H_{43}O_6N_4SCu]^+$	0.008	4.69E+06	✓
		27.90	698.21966	$[C_{34}H_{43}O_6N_4SCu]^+$	-0.062	4.61E+06	✓
		28.00	672.25809	$[C_{33}H_{45}O_7N_4Cu]^+$	-0.022	1.74E+06	✓
		28.25	652.23194	$[C_{33}H_{41}O_6N_4Cu]^+$	-0.002	9.38E+05	✗
		28.20	682.18843	$[C_{33}H_{39}O_6N_4SCu]^+$	0.008	4.27E+05	✗
		28.00	654.24751	$[C_{33}H_{43}O_6N_4Cu]^+$	-0.012	3.67E+05	✓
		27.95	942.39507	-	0.038	3.61E+05	✗
		28.10	972.40566	-	0.028	3.49E+05	✓
		28.15	714.21452	$[C_{34}H_{43}O_7N_4SCu]^+$	0.008	2.13E+05	✓
28.95	**33.34**						
		28.95	672.25822	$[C_{33}H_{45}O_7N_4Cu]^+$	-0.012	5.15E+06	✓
		28.90	654.24765	$[C_{33}H_{43}O_6N_4Cu]^+$	0.008	1.55E+06	✓
		29.00	1062.53595	-	-0.032	9.18E+05	✓
		28.85	1080.54657	-	0.038	2.48E+05	✓
		28.75	1064.55093	-	-0.022	2.33E+05	✓
30.79	**7.72**						
		29.55	767.27394	$[C_{41}H_{46}O_6N_5Cu]^+$	-0.002	4.72E+05	✓
		29.40	888.37356	-	-0.022	4.49E+05	✗
		30.00	1064.55176	-	-0.292	1.80E+05	✓
		30.40	759.21840	$[C_{35}H_{46}O_6N_5S_2Cu]^+$	-0.002	1.35E+05	✓

	30.30	632.20566	$[C_{33}H_{37}O_5N_4Cu]^+$	-0.012	8.03E+04	✗
	31.35	648.18280	-	0.048	6.19E+04	✗

Supplementary Table 4. Assignment fit for Cu ligands with predicted molecular formulae using Thermo Freestyle, using data from the 21T FT-ICR-MS**. Assignment Error** is calculated as the difference between measured *m/z* and theoretical *m/z*. **Cu Isotope Error** refers to the difference between the measured Δ*m/z* for Cu isotopes and 1.998192, the exact Δ*m/z*. **S Fit** is a spectral similarity score between the measured and theoretical isotope patterns calculated by Freestyle, and **Matched Isotopes** gives the number of peaks in the measured isotope pattern that match the theoretical isotope pattern. **MS Coverage** is calculated as the summed intensity of matched isotope peaks divided by the summed intensity of the measured pattern, while **Isotope Pattern Coverage** is the summed intensity of matched isotope peaks divided by the summed intensity of the theoretical pattern. Finally, **Combined Score** is another similarity score between measured and theoretical spectra but as a percentage. LC-ESI-MS refers to analysis on the Q Exactive Orbitrap, which is comparable to the chromatography in our LC-ICP-MS analyses, while FT-ICR-MS refers to analysis at the 21T facility (Methods).

These scores are reported to demonstrate a high degree of confidence in these formula assignments. Assignment errors were all below 1 ppm and averaged 0.40 ppm The most common reason for a lower combined score or other metric was a missing heavy isotopologue peak due to an overall lower intensity relative to the most abundant ions. Despite this, the high resolving power of the 21T FT-ICR-MS, relatively low assignment errors, low Cu isotope errors, and similarity of formulae with similar retention times gave high confidence to this analysis.

LC-ESI-MS Retention Time (min)	FT-ICR-MS^3 Mass-to-Charge (m/z)	Predicted Molecular Ion Formula	Assignment Error (ppm)	Cu Isotope Error (mDa)	S Fit	Matched Isotopes (#)	MS Coverage (%)	Isotope Pattern Coverage (%)	Combined Score
23.85	529.16326	$[C_{26}H_{32}O_5N_3Cu]^+$	0.01	-0.022	48.38	12	77.81	97.94	75.30
30.30	632.20566	$[C_{33}H_{37}O_5N_4Cu]^+$	0.33	-0.012	47.07	7	80.52	98.70	78.86
26.46	650.21622	$[C_{33}H_{39}O_6N_4Cu]^+$	0.33	-0.002	30.12	17	92.78	98.50	89.68
28.25	652.23194	$[C_{33}H_{41}O_6N_4Cu]^+$	0.43	-0.002	48.92	14	42.51	97.13	42.08
28.00	654.24751	$[C_{33}H_{43}O_6N_4Cu]^+$	0.30	-0.012	33.89	19	94.26	99.59	92.18
25.59	654.24755	$[C_{33}H_{43}O_6N_4Cu]^+$	0.37	-0.012	34.42	6	50.95	95.65	50.13
28.90	654.24765	$[C_{33}H_{43}O_6N_4Cu]^+$	0.51	0.008	54.68	14	92.14	98.62	89.42
26.20	664.19569	$[C_{33}H_{37}O_7N_4Cu]^+$	0.63	0.028	35.46	17	79.45	99.50	77.64
25.80	668.22670	$[C_{33}H_{41}O_7N_4Cu]^+$	0.19	0.008	40.48	17	95.67	99.09	92.86
24.30	670.24285	$[C_{33}H_{43}O_7N_4Cu]^+$	0.92	0.018	45.17	19	97.05	99.89	95.40
28.00	672.25809	$[C_{33}H_{45}O_7N_4Cu]^+$	0.31	-0.022	41.53	17	95.86	99.09	93.00
28.95	672.25822	$[C_{33}H_{45}O_7N_4Cu]^+$	0.51	-0.012	65.79	14	88.62	94.79	85.40
26.55	680.22677	$[C_{34}H_{41}O_7N_4Cu]^+$	0.29	-0.002	39.48	16	81.42	97.15	78.15
28.20	682.18843	$[C_{33}H_{39}O_6N_4SCu]^+$	0.50	0.008	27.43	27	92.00	99.20	89.41
27.10	682.24243	$[C_{34}H_{43}O_7N_4Cu]^+$	0.29	0.008	19.38	13	36.51	99.09	37.09
26.40	684.20469	$[C_{33}H_{41}O_6N_4SCu]^+$	0.69	-0.012	42.66	6	82.65	94.48	79.64
26.15	684.25814	$[C_{34}H_{45}O_7N_4Cu]^+$	0.38	-0.012	47.61	10	83.38	98.03	80.74
17.90	685.28562	$[C_{29}H_{48}O_8N_7Cu]^+$	0.19	-0.012	25.48	15	94.74	98.06	91.71
25.40	696.22161	$[C_{34}H_{41}O_8N_4Cu]^+$	0.17	-0.022	33.09	21	97.11	98.68	94.54
27.90	698.21966	$[C_{34}H_{43}O_6N_4SCu]^+$	0.31	-0.062	37.29	6	86.52	98.59	84.51
28.42	698.21969	$[C_{34}H_{43}O_6N_4SCu]^+$	0.44	0.008	48.36	4	55.94	93.59	54.36
21.25	698.23728	$[C_{34}H_{43}O_8N_4Cu]^+$	0.20	0.008	48.25	5	56.09	94.41	54.64
25.40	700.19892	$[C_{33}H_{41}O_7N_4SCu]^+$	0.12	-0.074	25.99	6	96.28	95.58	93.00
24.90	710.24853	$[C_{34}H_{43}O_7N_6Cu]^+$	0.22	0.018	28.54	14	89.21	98.25	86.66
28.15	714.21452	$[C_{34}H_{43}O_7N_4SCu]^+$	0.31	0.008	34.05	11	90.70	93.31	87.33
24.75	714.21466	$[C_{34}H_{43}O_7N_4SCu]^+$	0.51	0.008	40.69	6	62.43	97.66	61.25
27.30	716.23037	$[C_{34}H_{45}O_7N_4SCu]^+$	0.58	-0.002	26.56	8	81.07	99.34	79.96
20.27	728.24809	$[C_{35}H_{45}O_9N_4Cu]^+$	0.52	-0.002	40.14	18	92.52	97.18	89.98
25.40	731.23770	$[C_{37}H_{42}O_7N_5Cu]^+$	0.31	-0.012	60.03	13	92.98	97.76	89.92
30.40	759.21840	$[C_{35}H_{46}O_6N_5S_2Cu]^+$	0.52	-0.002	44.18	12	90.30	98.07	87.36
29.55	767.27394	$[C_{41}H_{46}O_6N_5Cu]^+$	0.10	-0.002	34.74	5	55.63	98.00	55.51
24.80	800.26901	$[C_{38}H_{49}O_{11}N_4Cu]^+$	0.22	-0.012	34.47	19	84.05	96.31	81.30
		MEAN	**0.37**		**39.51**		**80.91**	**97.54**	**78.72**
		STANDARD DEVIATION	**0.19**		**10.41**		**17.21**	**1.83**	**16.38**

Supplementary Table 5. **CLE-ACSV experimental setup.** Fe titration additions, aliquot volumes, and other voltammetry parameters are given for each sample.

	Sample ID	Aliquot Volume (µL)	Salicylaldoxime (SA) concentration (µM)	Fe titration additions (nM)	Deposition time (s)	Quiet time (s)
Iron	**MN19**	15	5	0, 0, 1, 2, 3, 5, 7.5, 10, 15, 20, 30, 40, 50, 75, 100	30	15
	MN20	40	5	0, 0, 0.5, 1.5, 2, 3, 4, 5, 7.5, 10, 15, 20, 30, 40, 50	60	15
	CRC7	40	5	0, 0, 0.5, 1.5, 2, 3, 4, 5, 7.5, 10, 15, 20, 30, 40, 50	60	15
	CRC210	15	5	0, 0, 1, 2, 3, 5, 7.5, 10, 15, 20, 30, 40, 50, 75, 100	30	15
	MSS1	15	5	0, 0, 1, 2, 3, 5, 7.5, 10, 15, 20, 30, 40, 50, 75, 100	30	15
Copper	**Sample ID**	**Aliquot Volume (µL)**	**Salicylaldoxime (SA) concentration**	**Cu titration additions (nM)**	**Deposition time (s)**	**Quiet time (s)**
	MN19	15	5	0, 0, 1, 2, 3, 5, 7.5, 10, 15, 20, 30, 40, 50, 75, 100	60	15
	MN20	40	5	0, 0, 1, 2, 3, 5, 7.5, 10, 15, 20, 30, 40, 50, 75, 100	120	15

Supporting Figures

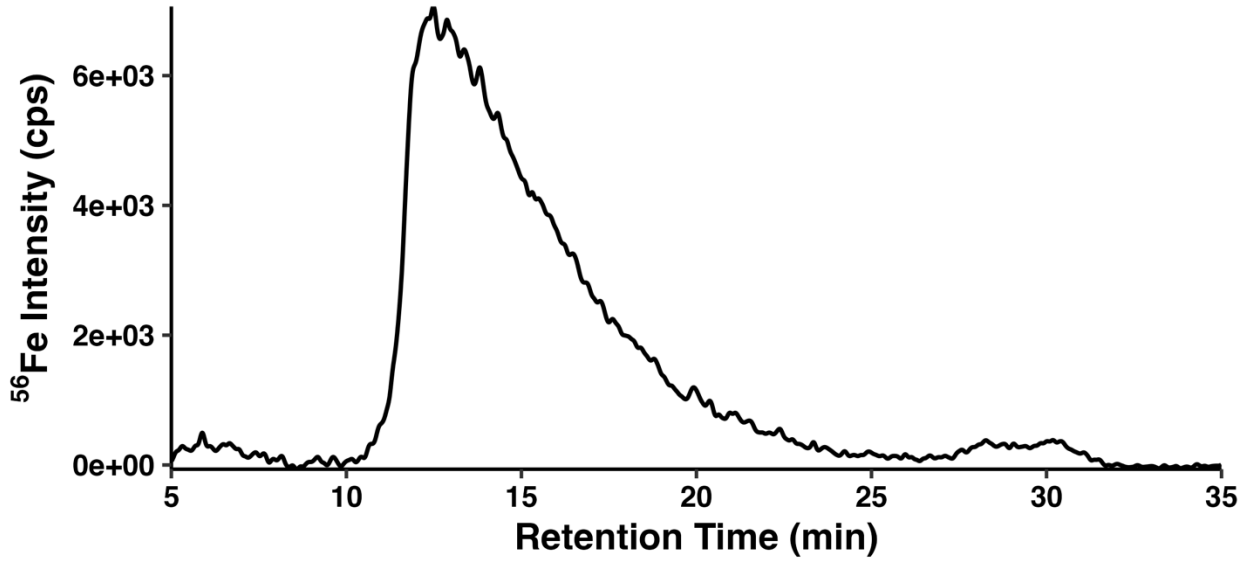

Supplementary Fig. 1. Example chromatogram for sample MN19. Baseline-corrected ^{56}Fe LC-ICP-MS chromatogram of sample MN19, showing the prominence of a chromatographically-unresolved group of ligands from 10–20 minutes. Ligands with metallophore-like properties in significant concentrations would come out as discrete peaks, as in the ^{63}Cu chromatogram of the Main Text (Fig. 2A), and therefore siderophores are likely not significant portions of the Fe ligand pool in whale fecal excrement. The large hump in the chromatogram, in conjunction with the subtle peak around -0.6 V in the voltammograms (Supplementary Fig. 2), suggested the presence of EPS or humic-like substances. This feature is also observed in the ^{63}Cu LC-ICP-MS chromatogram (Fig. 2A), demonstrating this is a relevant ligand class for Fe and Cu.

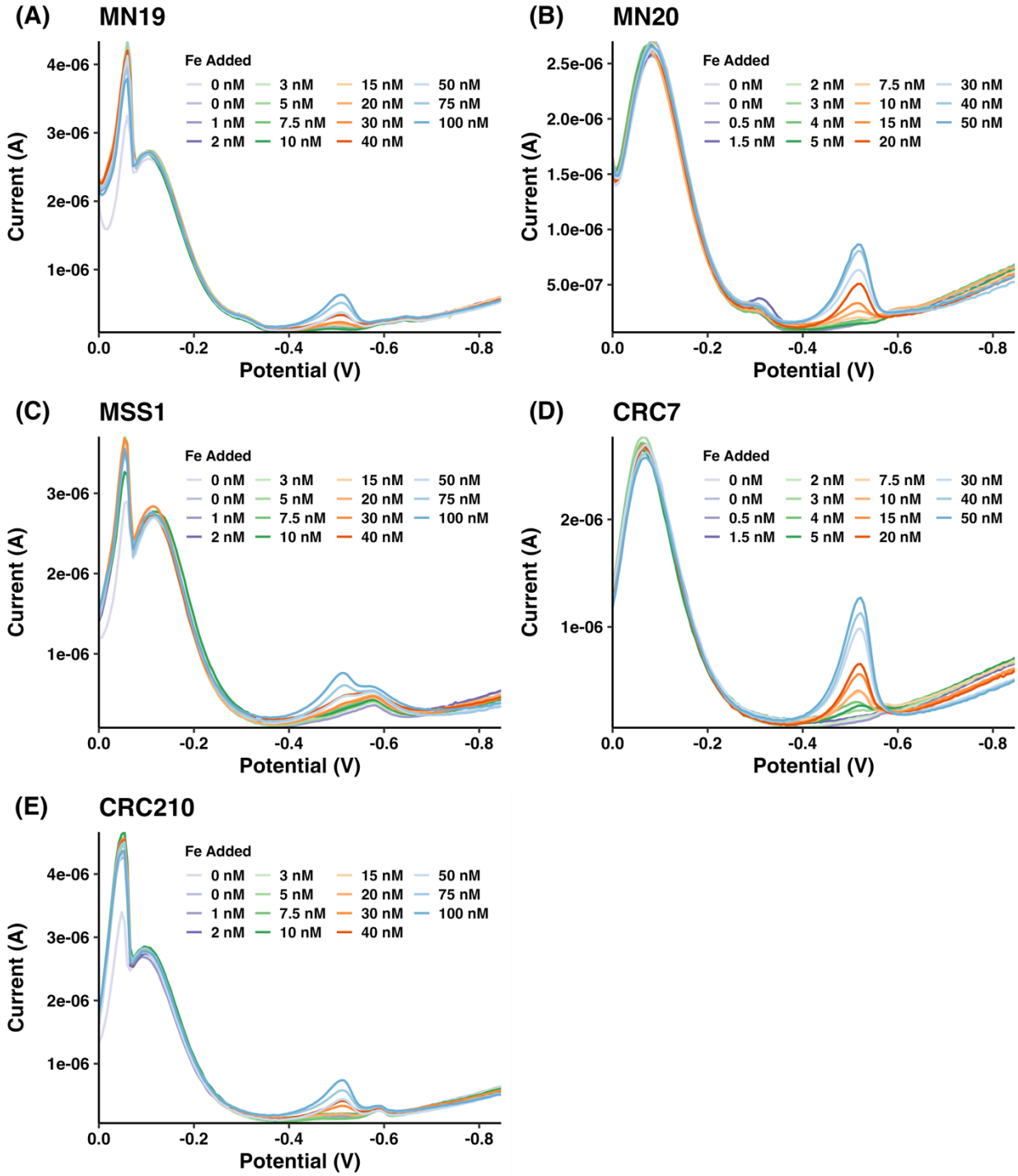

Supplementary Fig. 2. Voltammograms from Fe ligand analyses with CLE-ACSV. Methods for CLE-ACSV are explained in the main text. Peaks in current correspond to various complexes in the sample, with the peaks at -0.5 V and -0.6 V representing the Fe complexes with added ligand salicylaldoxime (SA) and electroactive humic-like substances, respectively (most evident in Supplementary Fig. 2E).

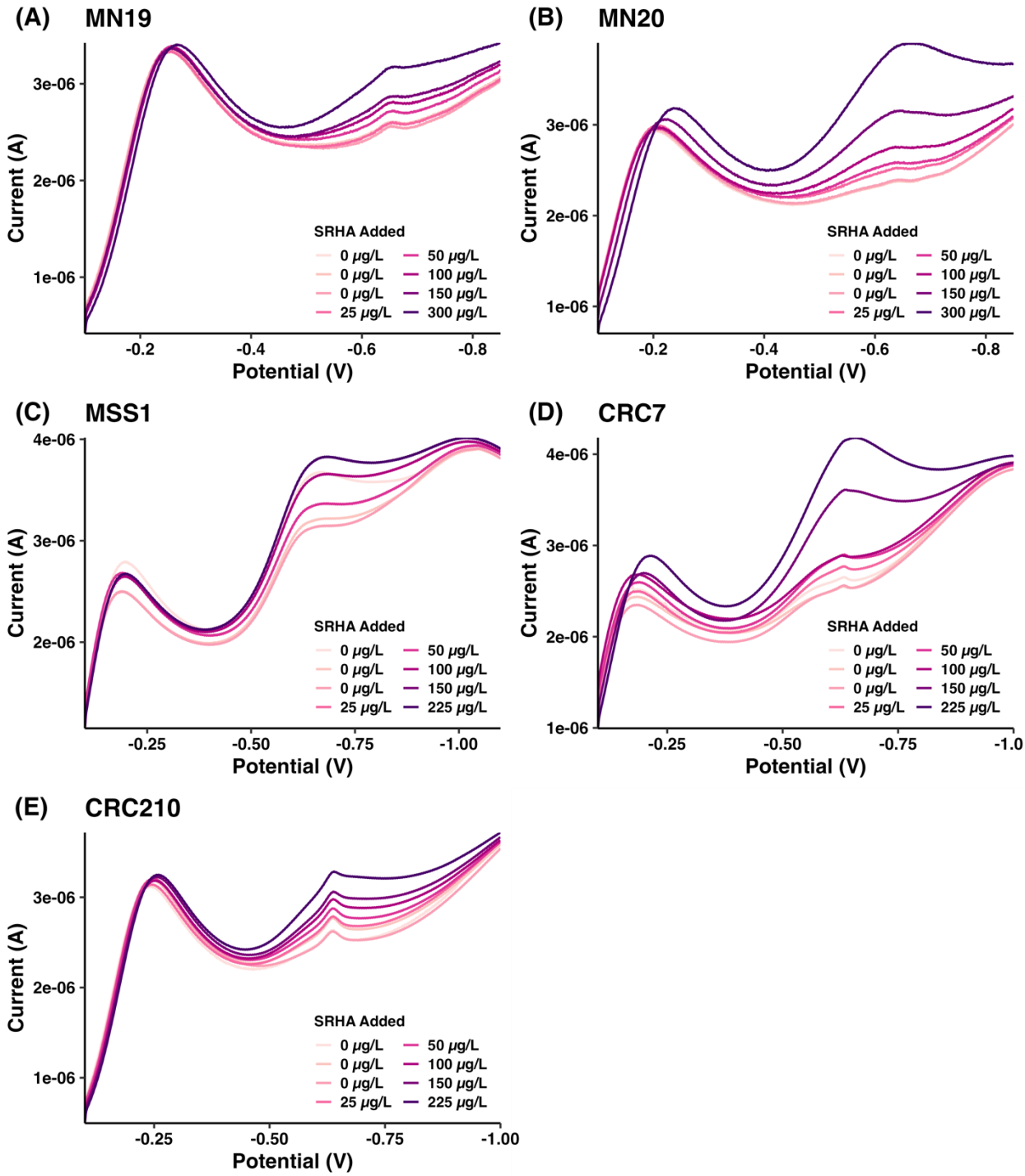

Supplementary Fig. 3. Voltammograms from standard addition of humic acid standard. Electroactive humic-like substances (eHS) were quantified according to Laglera et al. (2007)[4] in the Fe-ligand pool of all five fecal samples. The mercury drop electrode was operated in linear sweep mode at a -0.1 V deposition potential, 50 mV/s scan rate, and 180 s deposition time. [eHS] was calculated from a standard addition curve of Suwannee River Humic Acid (SRHA) Standard III using peak areas and converted to an Fe equivalent based on the range of reported binding capacities of fulvic and humic acid standards from the Suwannee River[5–7].

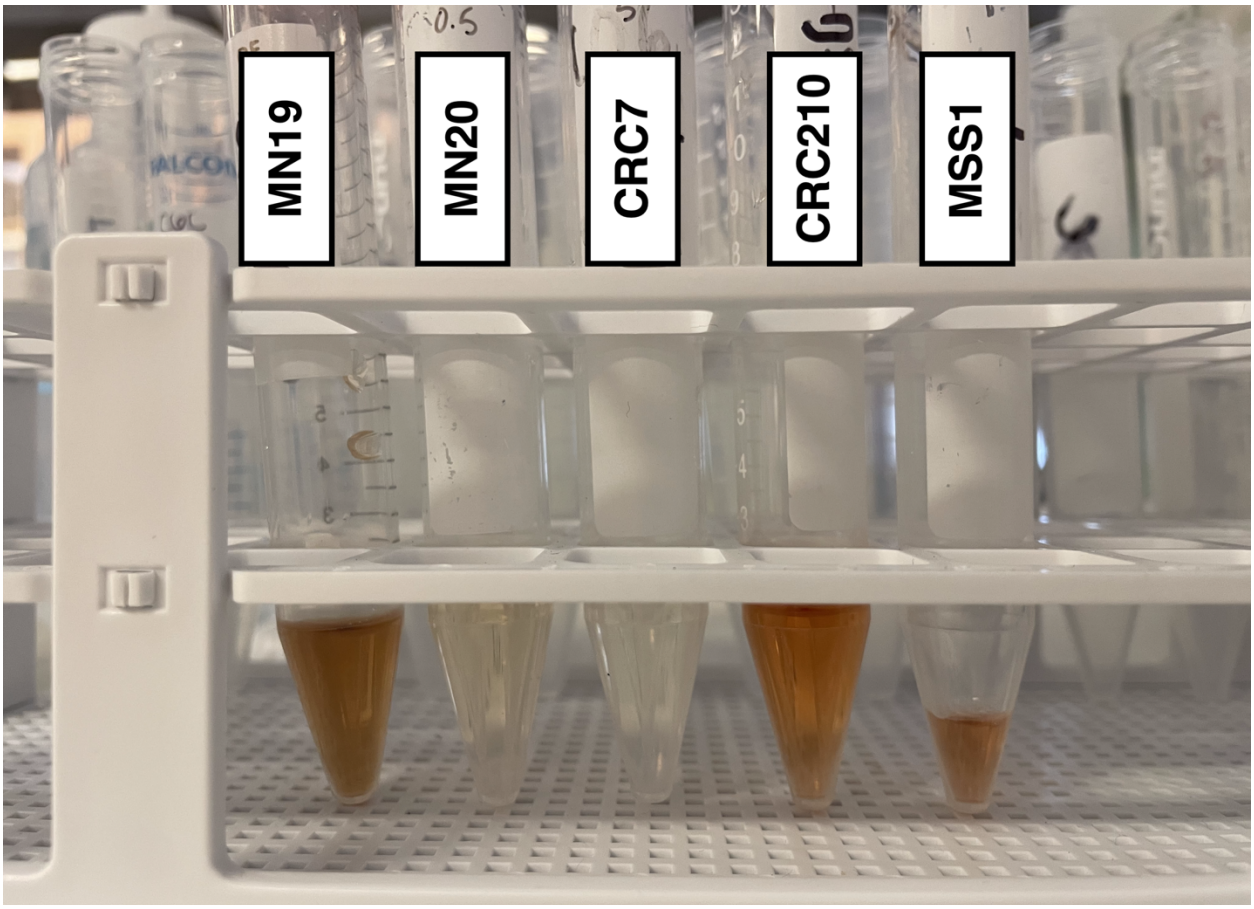

Supplementary Fig. 4. Photo of fecal filtrate. Samples were filtered through a 0.2-µm polycarbonate track-etch membrane filter (Pall Corporation) mounted on an acid-cleaned Teflon vacuum filtration rig (Savillex Corporation) in a HEPA-filtered laminar flow bench. Samples MN19 and MSS1 were dark brown, sample CRC210 was orange/brown, sample MN20 was light pink/orange and sample CRC7 was light pink/clear — in line with trends in trace metal content.

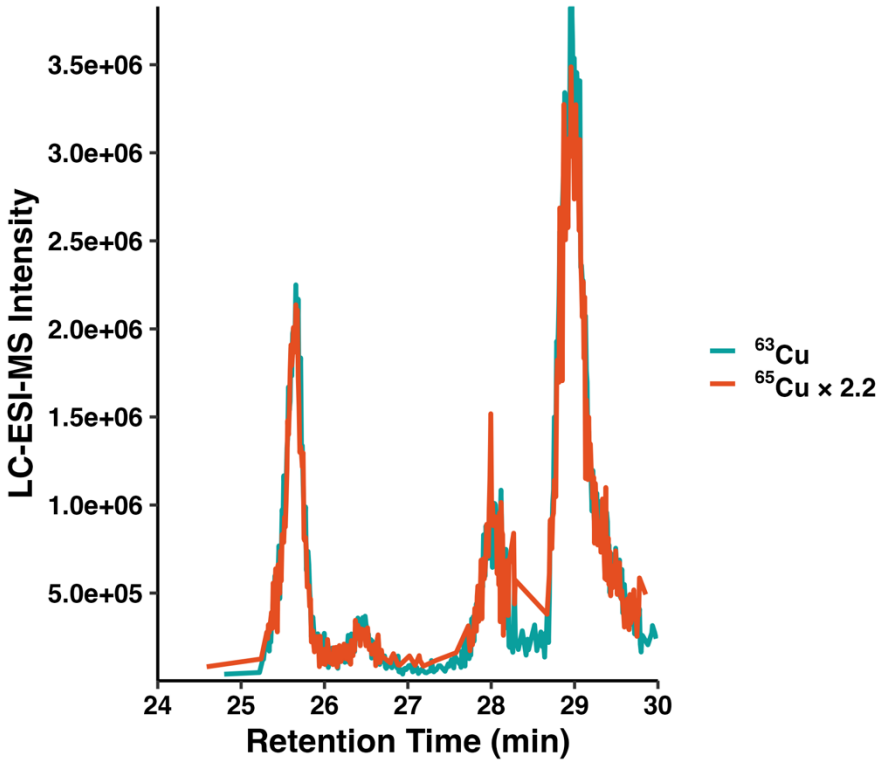

Supplementary Fig. 5. Extracted ion chromatogram (EIC) of Cu ligand *m/z* with multiple peaks. EICs for $[C_{33}H_{43}O_6N_4Cu]^+$ in sample MN19 (*m/z* = 654.24751 for ^{63}Cu-bound ligand and *m/z* = 656.24569 for ^{65}Cu-bound ligand) are plotted from LC-ESI-MS (Orbitrap) data. Intensities for the ^{65}Cu version of the ligand are scaled up by a factor of 2.2 according to the natural abundance ratio of ^{63}Cu/^{65}Cu, as in Fig. 2 of the main text. Close alignment of multiple peaks in EICs corresponding to ^{63}Cu and ^{65}Cu *m/z*'s suggest that isomers are present and common for Cu ligands. Cu ligands with multiple peaks have been observed in previous studies using similar methodologies[8,9]. EICs are plotted with a mass tolerance of 5ppm.

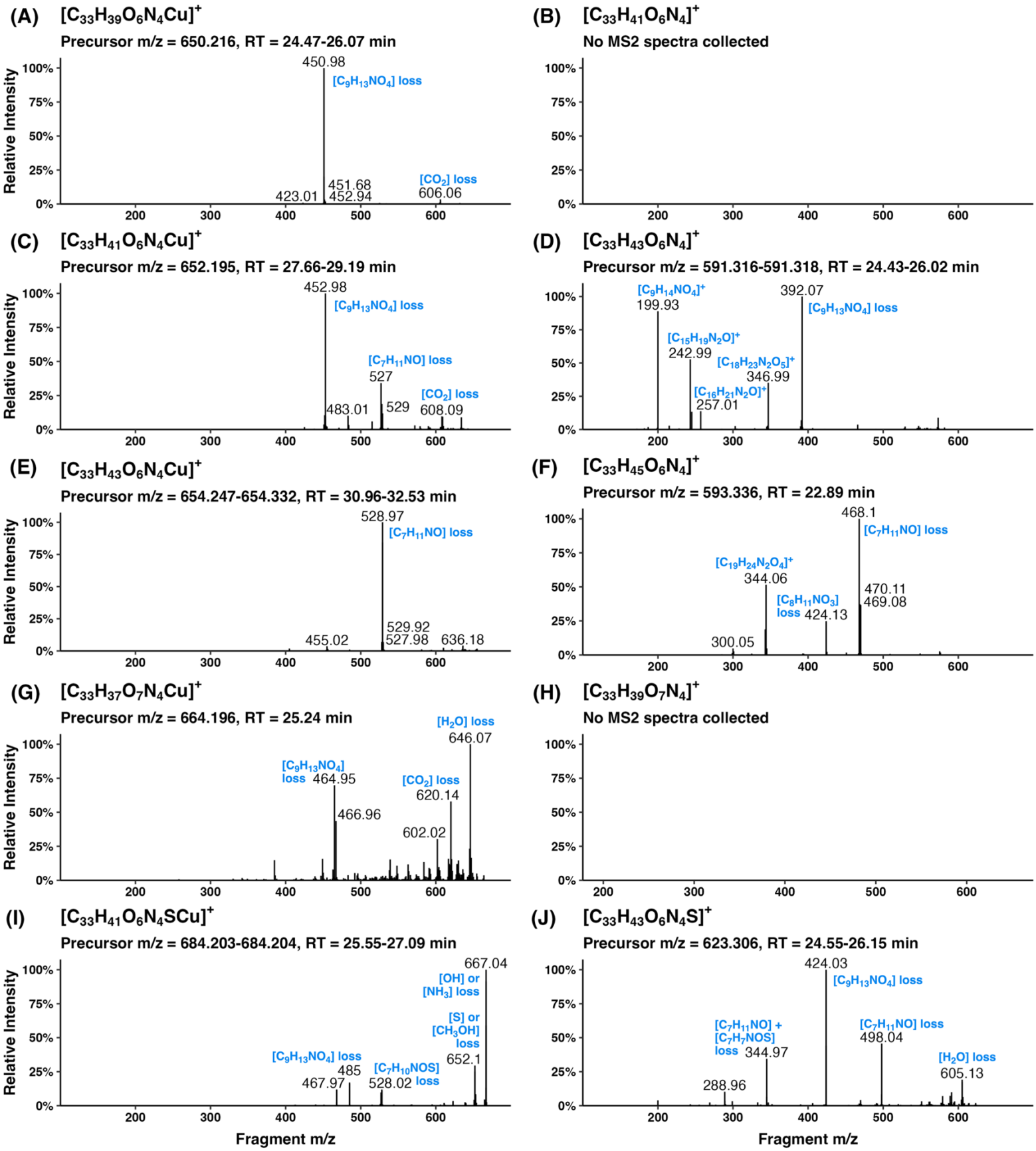
(A) [C33H39O6N4Cu]+
Precursor m/z = 650.216, RT = 24.47-26.07 min
450.98
[C9H13NO4] loss
423.01
451.68
452.94
[CO2] loss
606.06
(B) [C33H41O6N4]+
No MS2 spectra collected
(C) [C33H41O6N4Cu]+
Precursor m/z = 652.195, RT = 27.66-29.19 min
452.98
[C9H13NO4] loss
[C7H11NO] loss
527
483.01
529
[CO2] loss
608.09
(D) [C33H43O6N4]+
Precursor m/z = 591.316-591.318, RT = 24.43-26.02 min
[C9H14NO4]+
199.93
392.07
[C9H13NO4] loss
[C15H19N2O]+
242.99
[C18H23N2O5]+
346.99
[C16H21N2O]+
257.01
(E) [C33H43O6N4Cu]+
Precursor m/z = 654.247-654.332, RT = 30.96-32.53 min
528.97
[C7H11NO] loss
455.02
529.92
527.98
636.18
(F) [C33H45O6N4]+
Precursor m/z = 593.336, RT = 22.89 min
468.1
[C7H11NO] loss
[C19H24N2O4]+
344.06
[C8H11NO3] loss
424.13
470.11
469.08
300.05
(G) [C33H37O7N4Cu]+
Precursor m/z = 664.196, RT = 25.24 min
[H2O] loss
646.07
[C9H13NO4] loss
464.95
[CO2] loss
620.14
466.96
602.02
(H) [C33H39O7N4]+
No MS2 spectra collected
(I) [C33H41O6N4SCu]+
Precursor m/z = 684.203-684.204, RT = 25.55-27.09 min
667.04
[OH] or [NH3] loss
[S] or [CH3OH] loss
652.1
[C9H13NO4] loss
485
[C7H10NOS] loss
467.97
528.02
(J) [C33H43O6N4S]+
Precursor m/z = 623.306, RT = 24.55-26.15 min
424.03
[C9H13NO4] loss
[C7H11NO] + [C7H7NOS] loss
344.97
[C7H11NO] loss
498.04
[H2O] loss
605.13
288.96
Relative Intensity
Fragment m/z

Supplementary Fig. 6. MS2 spectra from select candidate Cu ligands in sample MN19. MS2 spectra were collected on the linear ion trap of the FT-ICR-MS system and processed using R package RaMS[10]. Similarities between molecular formulae to previously-published Cu ligand analyses[8,9] suggested that many of the ligands found in sample MN19 were linear tetrapyrroles, so MS2 spectra from masses with high concentrations were analyzed with *in-silico* fragmenter MetFrag[11] against known linear tetrapyrroles with identical formulae, like dinoflagellate luciferin and urobilinogen (Methods). Fragments of those known tetrapyrroles that matched those in the MS2 spectra are annotated in light blue. The purpose of this analysis was to do a cursory comparison of the fragment data using *in-silico* fragmentation of known compounds to propose potential molecular formula of Cu ligand fragment ions — not to perform in-depth and complete structural characterization.

The MS2 spectra of these ligands shared many abundant fragments. For example, losses of ~125 Da and ~199 Da dominated the spectra. Previous work on the fragmentation of bilin tetrapyrroles demonstrated loss of a terminal pyrrole group first[12]. The common fragments observed with these ligands could represent losses of a terminal pyrrole group, with 125 Da and 199 Da corresponding to $[C_7H_{11}NO]$ and $[C_9H_{13}NO_4]$, respectively, providing strong evidence that the masses belong to and are related to tetrapyrrole families. This analysis remains preliminary, as complete structural characterization was outside the scope of this work. Structures plotted with ChemDraw 21.0.0.

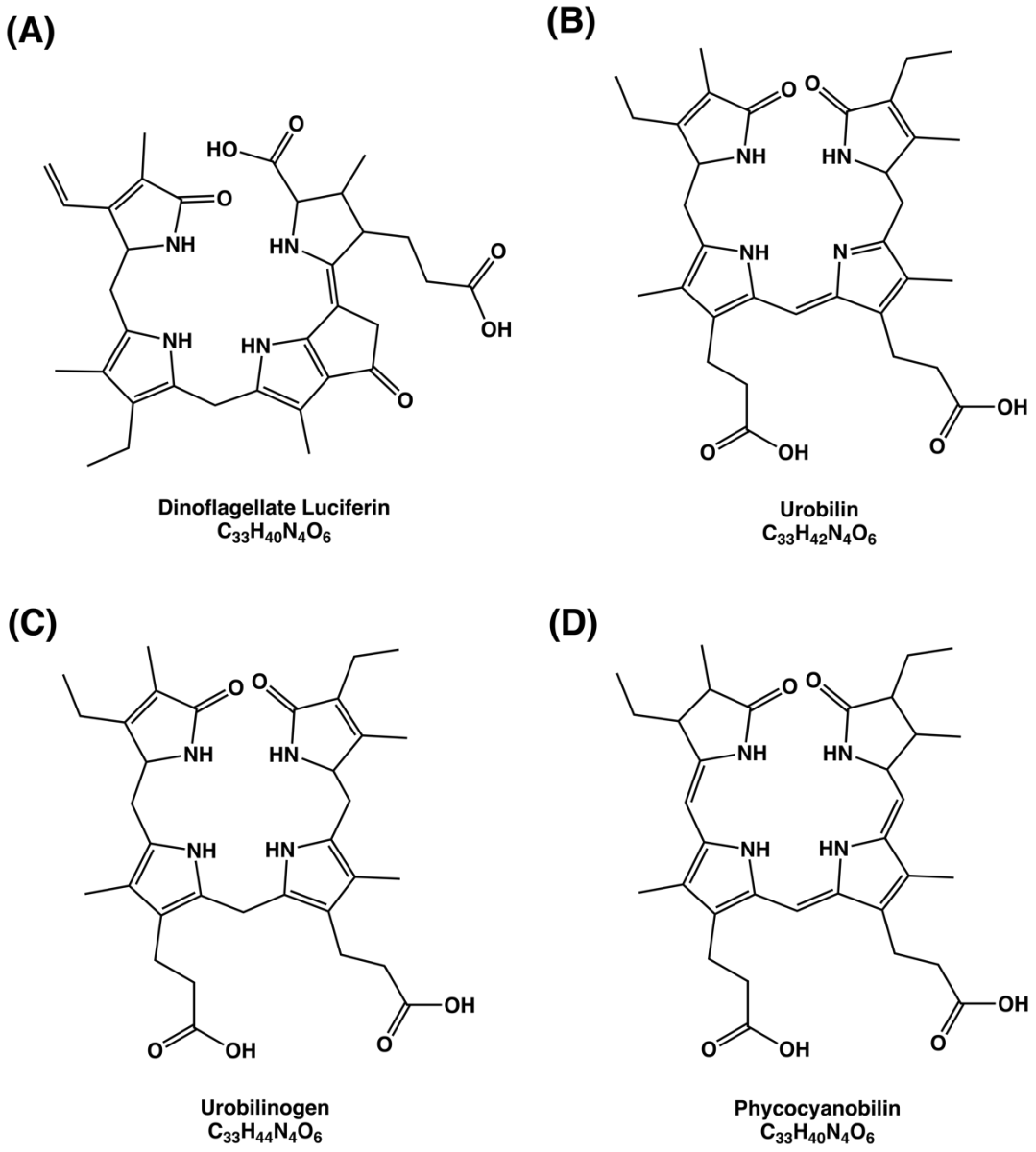

Supplementary Fig. 7. Linear tetrapyrrole example structures. Structures of known linear tetrapyrrole compounds that share molecular formulae with some of the Cu ligands found in fecal excrement are presented. It is likely that the Cu ligands in this study resemble or are related to these, which are heme and chlorophyll catabolites. These classes of compounds contain several similar molecules, which differ only in degrees of saturation, pyrrole substitution, placement of double bonds, or other slight modifications. Because of the overlap of many of these compounds, we are not able to resolve the exact structure, but many masses have multiple peaks in the LC-ESI-MS (Orbitrap) and LC-FT-ICR-MS data, suggesting isomers are present. Generated with ChemDraw 21.0.0.

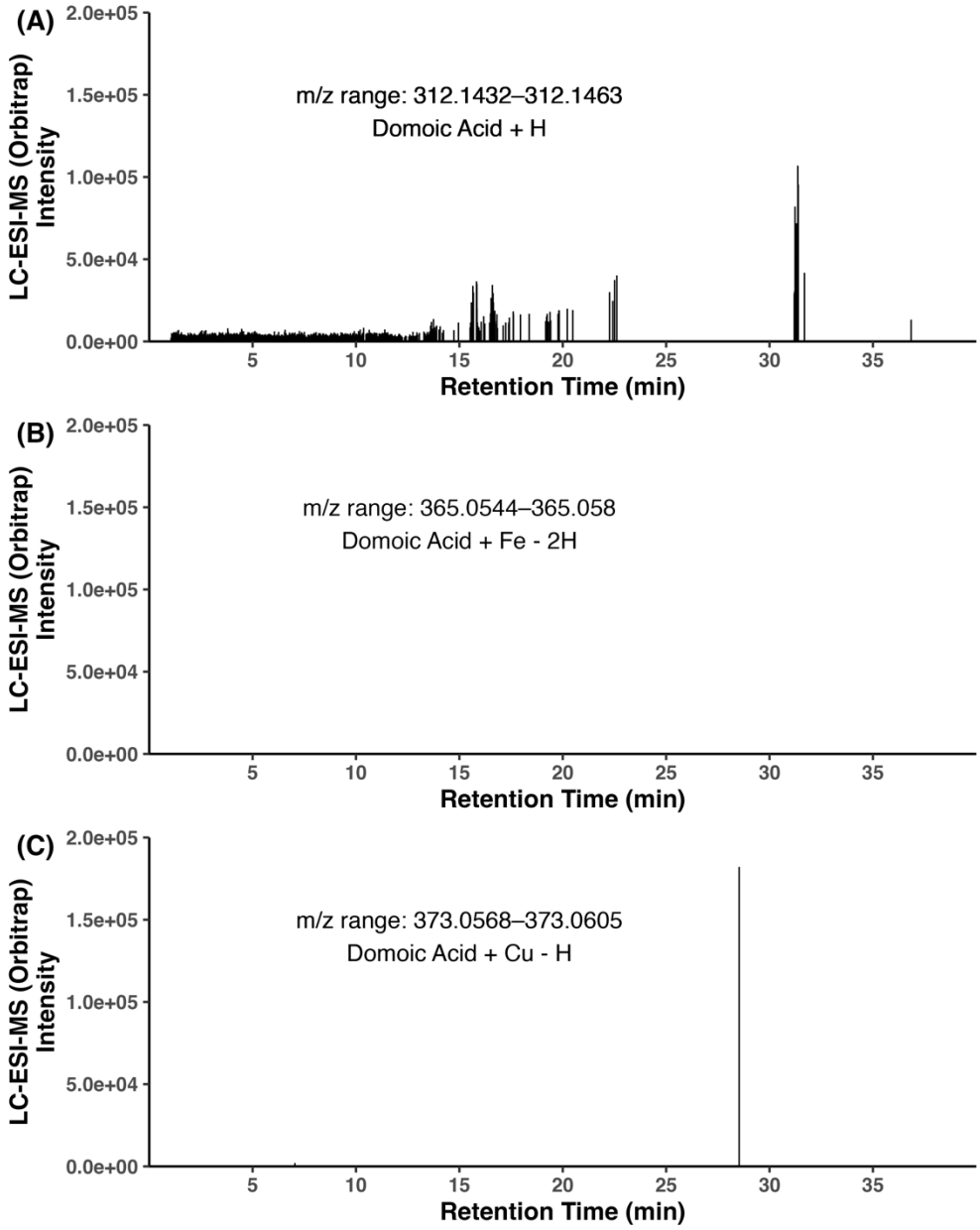

Supplementary Fig. 8. Extracted ion chromatograms (EICs) of domoic acid ion. Domoic acid has a binding strength that is remarkably similar to that of the L_4 Fe-ligand-pool detected here, so EICs from analyses on the Q Exactive Orbitrap for the hydrogen adduct for (A) domoic acid, (B) domoic acid bound to Fe(III), and (C) domoic acid bound to Cu(II) were plotted to see if domoic acid was present in our solid-phase extracted samples. No well-defined peaks were found (sodium and ammonium adducts were also checked, data not published), suggesting domoic acid either is too polar to be retained on the columns we used for solid-phase extraction (Methods) or was not present in the sample. Domoic acid is known to bioaccumulate up the food chain and has been detected in whale feces with other methods (see main text).

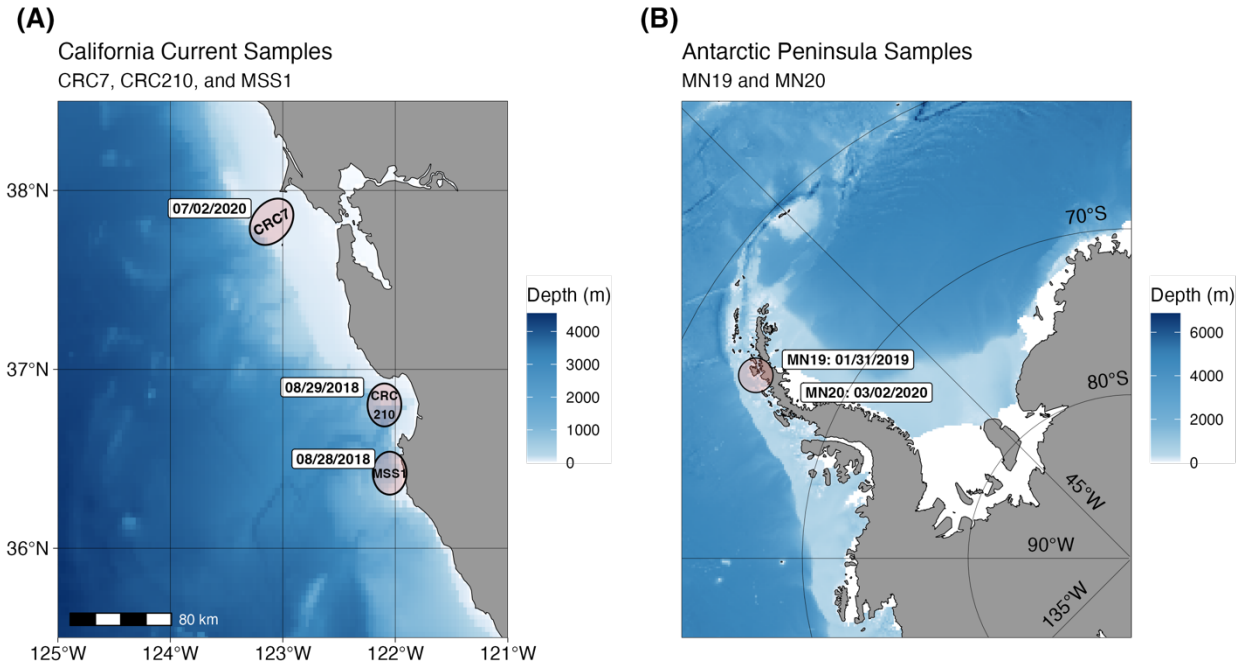

Supplementary Fig. 9. Map of sample collection areas. (A) Samples CRC7, CRC210, and MSS1 were collected from blue whales (*Balaenoptera musculus*) off the California coast. (B) Samples MN19 and MN20 were collected from humpback whales (*Megaptera novaeangliae*) in nearshore waters along the western side of the Antarctic Peninsula. Approximate sampling locations are indicated with a pink circle, with the date of sampling provided next to it. Samples were part of other projects examining whale ecophysiology and have been abbreviated in some instances for clarity and brevity. As such, MN19, MN20, CRC7, and CRC210 are also known as "Mn19_031E_P", "Mn20_062C_P", "CRC Sighting #7", and "CRC 20180829-210", respectively.

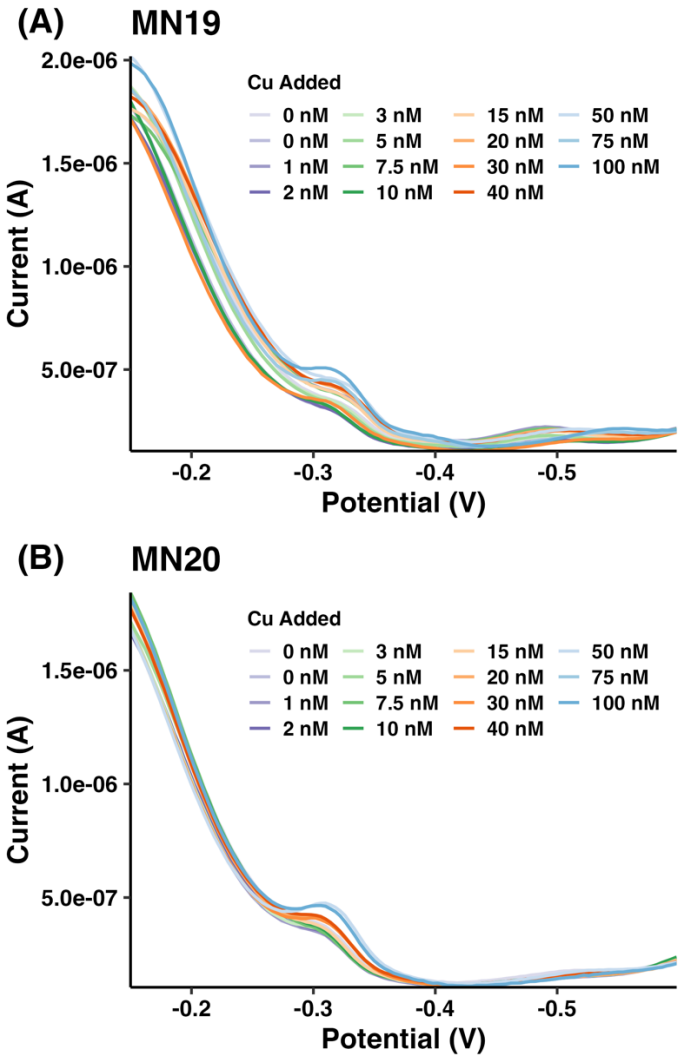

Supplementary Fig. 10. Voltammograms from Cu ligand analyses with CLE-ACSV. Methods for CLE-ACSV are explained in the main text. Peaks in current correspond to various complexes in the sample, with the peaks at -0.3 V representing the Cu complex with added ligand salicylaldoxime (SA). Due to sample availability, titrations were only performed on samples MN19 and MN20.

.

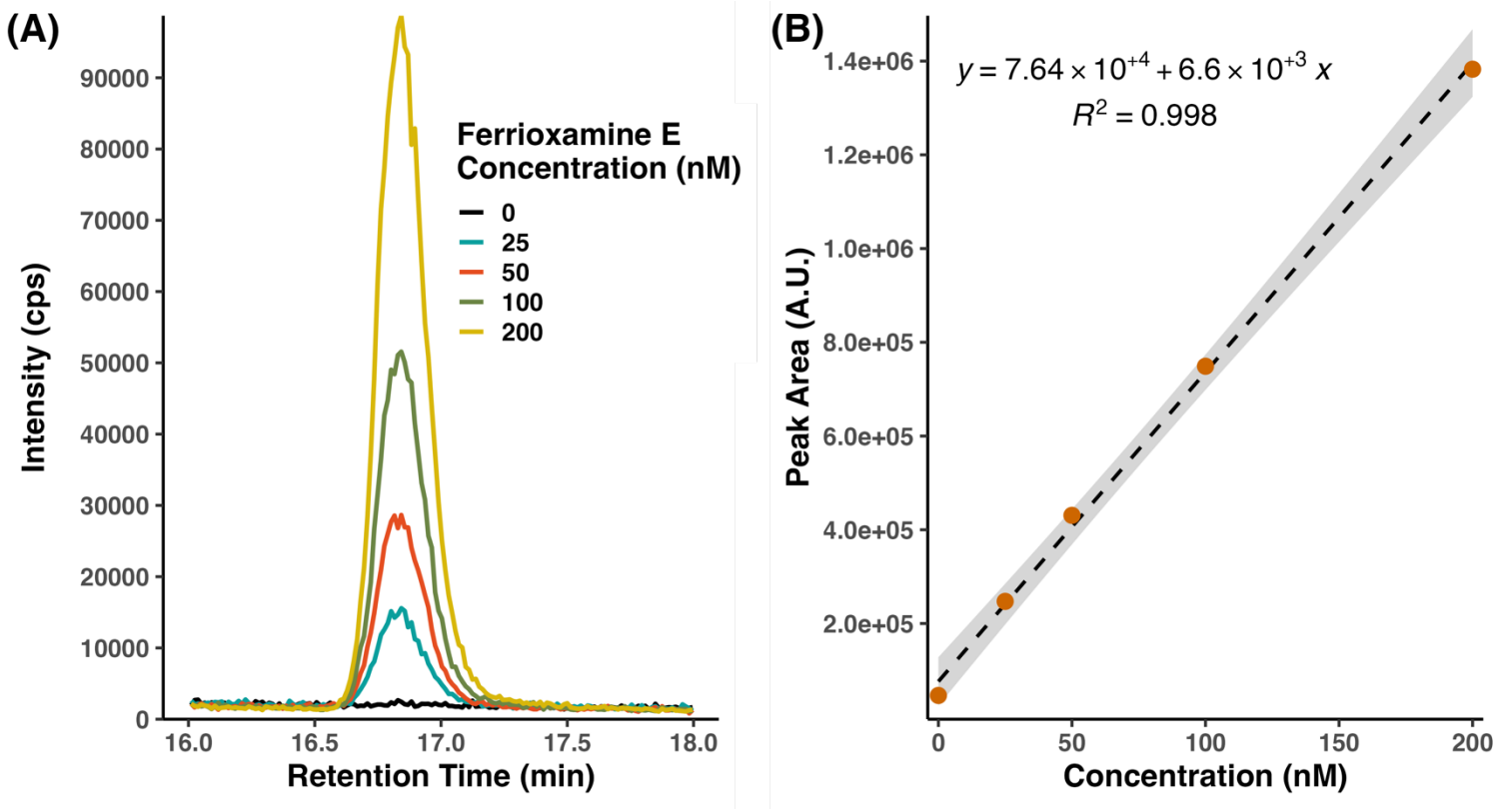

Supplementary Fig. 11. LC-ICP-MS Standard Curve. The standard curve for LC-ICP-MS analysis — used to calculate total SPE metal-bound ligand concentrations ($[Fe\text{-}L]_{SPE}$) and individual peak concentrations in Supplementary Table 2 — are presented as both (A) LC-ICP-MS Fe chromatograms of four ferrioxamine E solutions and a blank and (B) the analytical curve with peaks areas plotted against standard concentrations. The dotted line represents a Type I least-squares regression, and the shaded area is the 95% confidence interval of the model. The limit of detection of this analysis on SPE eluent, using $(3.3s_r)/m$, where s_r is the standard deviation about the regression and m is the slope of the regression curve, was 80 pM. Because the eluent was concentrated from 3-10 mL of sample, this corresponds to a limit of detection of 8–26 pM for sample concentrations.

References

1. Omanović, D., Garnier, C. & Pižeta, I. ProMCC: An all-in-one tool for trace metal complexation studies. *Mar. Chem.* **173**, 25–39 (2015).

2. Abualhaija, M. M. & van den Berg, C. M. G. Chemical speciation of iron in seawater using catalytic cathodic stripping voltammetry with ligand competition against salicylaldoxime. *Mar. Chem.* **164**, 60–74 (2014).

3. Bahureksa, W. *et al.* Improved Dynamic Range, Resolving Power, and Sensitivity Achievable with FT-ICR Mass Spectrometry at 21 T Reveals the Hidden Complexity of Natural Organic Matter. *Anal. Chem.* **94**, 11382–11389 (2022).

4. Laglera, L. M., Battaglia, G. & van den Berg, C. M. G. Determination of humic substances in natural waters by cathodic stripping voltammetry of their complexes with iron. *Anal. Chim. Acta* **599**, 58–66 (2007).

5. Laglera, L. M. & van den Berg, C. M. G. Evidence for geochemical control of iron by humic substances in seawater. *Limnol. Oceanogr.* **54**, 610–619 (2009).

6. Whitby, H. *et al.* A call for refining the role of humic-like substances in the oceanic iron cycle. *Sci. Rep.* **10**, (2020).

7. Sukekava, C., Downes, J., Slagter, H. A., Gerringa, L. J. A. & Laglera, L. M. Determination of the contribution of humic substances to iron complexation in seawater by catalytic cathodic stripping voltammetry. *Talanta* **189**, 359–364 (2018).

8. Babcock-Adams, L. Molecular Characterization of Organically Bound Copper in the Marine Environment. *Woods Hole Open Access Serv.* (2022). doi:10.1575/1912/28623

9. Babcock-Adams, L., Li, J., McKenna, A. M., Hendrickson, C. L. & Repeta, D. J. Detection and Structural Elucidation of Copper Binding Tri- and Tetrapyrrole Ligands Produced by the Marine Diatom Phaeodactylum tricornutum. *J. Am. Soc. Mass Spectrom.* **In Review**, (2024).

10. Kumler, W. & Ingalls, A. E. Tidy Data Neatly Resolves Mass-Spectrometry's Ragged Arrays. *R J.* **14**, 193–202 (2022).

11. Ruttkies, C., Schymanski, E. L., Wolf, S., Hollender, J. & Neumann, S. MetFrag relaunched: incorporating strategies beyond in silico fragmentation. *J. Cheminform.* **8**, (2016).

12. Quinn, K. D., Nguyen, N. Q. T., Wach, M. M. & Wood, T. D. Tandem mass spectrometry of bilin tetrapyrroles by electrospray ionization and collision-induced dissociation. *Rapid Commun. Mass Spectrom.* **26**, 1767–1775 (2012).